AGU PUBLICATIONS

JGR

Journal of Geophysical Research: Oceans

RESEARCH ARTICLE

10.1002/2014JC009825

Special Section:
Early scientific results from the salinity measuring satellites Aquarius/SAC-D and SMOS

The North Atlantic subtropical surface salinity maximum as observed by Aquarius

Frederick M. Bingham[1], Julius Busecke[2], Arnold L. Gordon[2], Claudia F. Giulivi[2], and Zhijin Li[3]

[1]Center for Marine Science, University of North Carolina Wilmington, Wilmington, North Carolina, USA, [2]Lamont Doherty Earth Observatory of Columbia University, Palisades, New York, USA, [3]Jet Propulsion Laboratory, California Institute of Technology, Pasadena, California, USA

Key Points:
- North Atlantic surface salinity maximum documented from August 2011 to September 2013
- Aquarius satellite sea surface salinity data are used
- Feature shows long-term fluctuations and documents seasonal variability

Correspondence to:
F. M. Bingham,
binghamf@uncw.edu

Citation:
Bingham, F. M., J. Busecke, A. L. Gordon, C. F. Giulivi, and Z. Li (2014), The North Atlantic subtropical surface salinity maximum as observed by Aquarius, *J. Geophys. Res. Oceans*, *119*, 7741–7755, doi:10.1002/2014JC009825.

Received 15 JAN 2014
Accepted 17 OCT 2014
Accepted article online 24 OCT 2014
Published online 19 NOV 2014
Corrected 2 FEB 2015

This article was corrected on 2 FEB 2015. See the end of the full text for details.

Abstract Aquarius satellite-derived sea surface salinity (SSS) data from August 2011 through September 2013 reveals significant seasonal migration and freshening of the subtropical surface salinity maximum (SSS-max) area in the North Atlantic, in good agreement with in situ observations, including those obtained as part of the SPURS (Salinity Processes in the Upper Ocean Regional Study) field experiment in 2012–2013. The SSS-max fluctuated in surface area—as defined by the 37.4 surface isohaline—during the course of the Aquarius time series by about 67%. The SSS-max has a surprisingly large amount of non-seasonal variability, including a general decrease in salinity throughout the eastern subtropical North Atlantic between 2011–2012 and 2012–2013 of about 0.1–0.2. The documented seasonal variability is weakest in the maximum salinity area and increases toward the north and south, respectively. This is consistent with the important role played by Ekman transport and regional excess of evaporation over precipitation in the formation of the SSS-max.

1. Introduction

The subtropical sea surface salinity maximum (SSS-max) is a ubiquitous feature of the surface ocean, found in every major basin. In the North Atlantic it is the origin and outcrop of the so-called subtropical underwater (STUW) [*O'Connor et al.*, 2005], the subsurface vertical salinity maximum found between 12°N and about 25°N in the upper 200 m [*Talley et al.*, 2011]. This water mass is the poleward end of the subtropical cell or shallow meridional overturning circulation [*McCreary and Lu*, 1994; *Zhang et al.*, 2003] that transmits high salinity water into the upper part of the tropical Atlantic which then returns at the surface. It can be defined by a closed sea surface salinity (SSS) contour whose value might be different in every ocean. For the North Atlantic we take that value to be 37.4 for convenience. Lower values tend to impinge on the coast and higher values can disappear at times. The results we will show do not depend much on which isohaline is chosen.

Until now, the SSS-max has not been a subject of intensive study. Its general presence has been known for decades [*Worthington*, 1976], but only through observations widely spaced in time, with little knowledge of its structure or variability. There have been observations of it using thermosalinograph (TSG) measurements from volunteer ships [*Dessier and Donguy*, 1994; *Reverdin et al.*, 2007]. Though these measurements have high along-track spatial resolution, they are on specific tracks and the time resolution is monthly at best and more typically quarterly. There are observations from Argo floats, which have a resolution of about one measurement 3° × 3° every 10 days [*Roemmich et al.*, 2001]. Finally, model results can give insight [*Qu et al.*, 2011, 2013; *Mourre et al.*, 2008] but need to be backed by observational evidence. The launch of the Aquarius satellite [*Lagerloef et al.*, 2008] gives us global along-track data that have a high spatial resolution and a 7 day repeat cycle to better understand the structure and variability of the SSS-max.

In 2012 and 2013, the SPURS (Salinity Processes in the Upper Ocean Regional Study) experiment was carried out in order to characterize the upper ocean processes that maintain the SSS-max and by inference those of other ocean basins. In the classical view [*Worthington*, 1976], it is maintained by a balance of northwestward Ekman transport at the surface driven by northeast trade winds in the 15°N–20°N band, subduction at the northern edge of the trades and an excess of evaporation over precipitation as the surface waters drift to the north. In addition there is Ekman transport of cool, fresh water from the north driven by midlatitude

westerly winds [*Gordon and Giulivi*, 2014, Figure 3]. *Qu et al*. [2013] emphasize the northern limb of this circulation, asserting that water in the SSS-max gets there from the northwestern part of the subtropical gyre, also having drifted southeastward through an area of high evaporation. The SPURS experiment has sought to fill in the details of the subduction process, upper ocean processes in the middle of the SSS-max, and the balance of terms controlling the salinity in the mixed layer. While the SPURS observations have not been fully analyzed yet, one insight gained is that this region is more energetic and has more fronts and eddies than previously thought [*Gordon and Giulivi*, 2014].

The Aquarius satellite and the in situ observations are different but highly complementary. TSGs installed on volunteer observing ships [*Reverdin et al*., 2007] make bulk (upper few meters), point measurements with high accuracy, ∼0.01 or better depending on the platform, and high spatial and temporal resolution but a long repeat time. Argo floats make point measurements with similar accuracy, but are relatively random and can be widely spaced. The satellite on the other hand measures skin salinity over a footprint of typically 100 km with much lower accuracy (∼0.3 over a month) [*Lagerloef et al*., 2013] but with a continuity that is not possible with in situ instruments. The SPURS experiment has studied the details of the SSS field in the SSS-max with intensive measurements in an attempt to bridge the gap between small and large scales [*Busecke et al*., 2014]. While considerable effort is being put into making sense of the in situ observations from SPURS, a similar effort needs to be carried out with the Aquarius data, keeping in mind the capability, accuracy, sampling characteristics, and footprint of the satellite measurements.

2. Data and Methods

The satellite data used in this paper come from the global Aquarius SSS data set, version 3.0. We used the level 2, swath-based data. Files were downloaded from the PO.DAAC Aquarius data archive (see Acknowledgements section for access to all data sets referred to in this paper). For this study, we used only data between 10°N and 35°N, binned, and averaged along track to 1/2° intervals between those latitudes.

The satellite has a 7 day repeat track of 103 orbits or about 15 orbits per day [*PO.DAAC*, 2014]. Each orbit has three beams. The final data set presented here contains about 105 one week repeat cycles, 737 days, or 10,833 orbits total. It spans the time period from 26 August 2011 to 31 August 2013. Each of the first 103 orbits defines a set of locations identified by beam number (three beams), repeat track (103 repeat tracks), ascending/descending (two states), and latitude/longitude (fifty 1/2° bins, centered at 10.25°N–34.75°N). In this paper we use eight of the repeat tracks that pass through the SPURS region (15°N–30°N, 30°W–45°W; Figure 1), four ascending and four descending. For clarity, we call each of these (3*8*2*50=) 2400 points a node. At each node, a time series of SSS can be formed with about 105 values, one for each repeat cycle or week. The nodes are relatively evenly distributed in latitude and longitude over the ocean between 10°N and 35°N, though the distribution is not completely uniform. The level 2 swath-based data were used rather than level 3 gridded to avoid extraneous smoothing tying adjacent nodes to each other and to be able to get some sense of the along-track fronts and the presence of mesoscale variability. Each node time series becomes an independent set of measurements. No quality control was done on the Aquarius salinity data for this paper beyond a gross range check, check for land proximity (eliminating 2 of the 2400 nodes, those that contain the Cape Verde Islands) and a check for consistent orbital position. The orbits, beams, nodes and mean salinity in Figure 1 show the extent of coverage of the area. Remembering that each footprint is approximately an ellipse with 100 km major axis [*Lagerloef et al*., 2008; *PO.DAAC*, 2014] that coverage is mostly complete.

At each node a time series was formed and used in a harmonic analysis to obtain the amplitude and phase of the seasonal cycle. For details of the method used to get annual harmonics see *Emery and Thomson* [2001, pp. 392–395] and *Bingham et al*. [2010, section 2.2]. In this study all seasonal amplitudes and phases are displayed, with no attempt to determine statistical significance. One must remember when doing harmonic analysis on the Aquarius data that only two realizations of the seasonal cycle have been sampled and thus the results should be considered preliminary.

As Aquarius is the first instrument deployed by NASA specifically to measure global SSS and one of the first attempts to measure SSS from space at all, it is important to understand its strengths and limitations. The report by *Lagerloef et al*. [2013] details the accuracy of the Aquarius retrievals for the 2.0 version. (It should be noted here that in this paper we use the 3.0 version of the data set, which has some considerable improvements in accuracy over the 2.0 (G. Lagerloef, personal communication, 2013). A similar report for

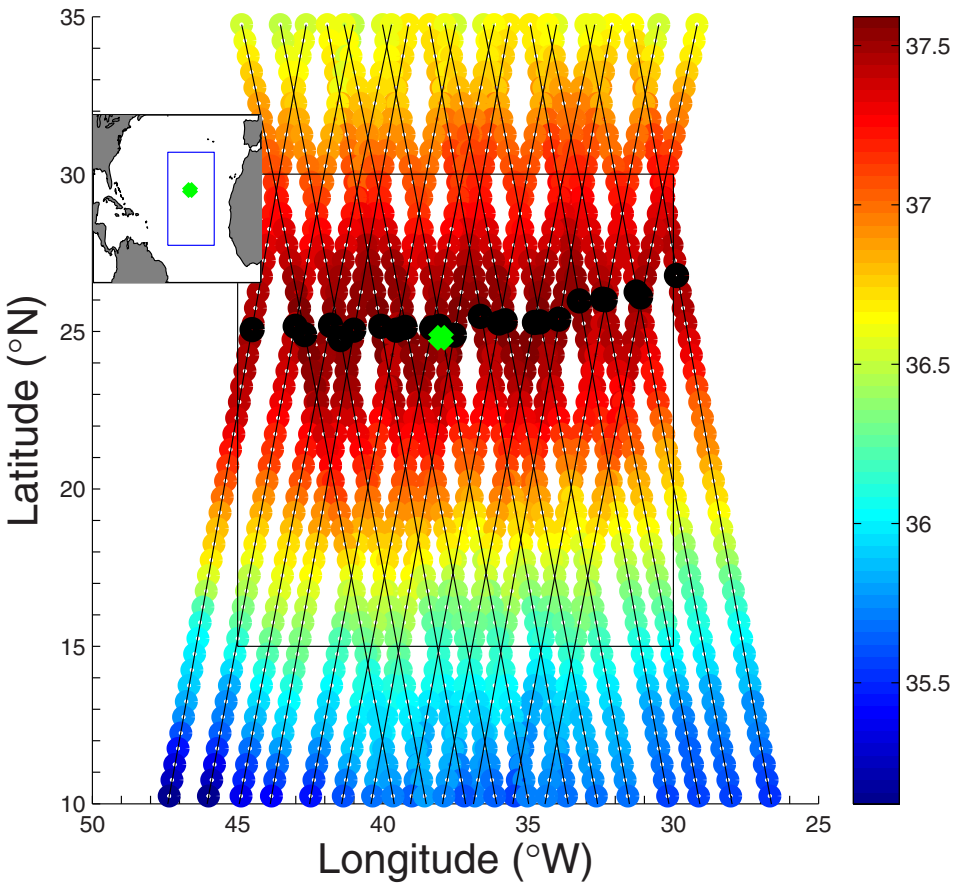

Figure 1. Ground paths of the Aquarius satellite tracks used in this study in the North Atlantic (slanted black lines). There are four ascending (southeast-northwest) and four descending (northeast-southwest) tracks, each with three beams for a total of 24 lines. The SPURS region (15°N–30°N, 30°W–45°W) is outlined as a black rectangle. Colored symbols indicate mean salinity over the time period August 2011 to September 2013 for each particular node. Black symbols are the mean location of the maximum salinity for a particular track and beam. Green symbol is the location of the SPURS central mooring (Figure 2). Note that the colored symbols are about half the size of the typical Aquarius footprint. Inset indicates location of plotbox (blue) in the North Atlantic with green symbols corresponding in location between figure and inset.

the 3.0 data were not available as of the date this paper was submitted for publication.) The Aquarius data set is most problematic at low sea surface temperature where the sensitivity of brightness temperature to conductivity is weak, close to land, and in areas of high surface roughness [*Lagerloef et al*., 2008]. Since the region of the SSS-max does not meet any of those criteria, it is an ideal location to make use of it. The stated RMS error in the *Lagerloef et al*. [2013] report for the level 3 2.0 version at 150 km × 150 km length scales and monthly time scales is 0.3. (No such number is stated for the level 2 data used in this study.) This number includes more problematic areas, so one would expect the error to be smaller than that in a region like the SSS-max. Y. Chao (personal communication, 2014) using SPURS in situ data for validation reports a much lower RMS error in this region of 0.16 using level 2 version 3.0 Aquarius data. *Busecke et al*. [2014] capture SSS signals in this region well below the 0.3 stated accuracy as well [*Busecke et al*., 2014, Figure 6]. The *Lagerloef et al*. [2013] report does urge users to exercise caution in interpreting annual signals in the data, an urging which we pass along to the readers of this paper. However, this caveat is given mainly for the southern hemisphere and at high latitudes, neither of which apply to the SSS-max region. Of course as the Aquarius data set is new and relatively untested it is possible that a newer and better version of it could eventually render questionable or invalid the results shown here. However, as we will see, the basic structure of the SSS-max and its seasonal variability agree with previous observations, giving confidence that other results that are more difficult to validate are reasonable.

A few other data sets are mentioned briefly in this paper. SSS from the SPURS central mooring (Figure 1) come from a depth of less than 1 m. Ships of opportunity program (SOOP) TSG data were collected and

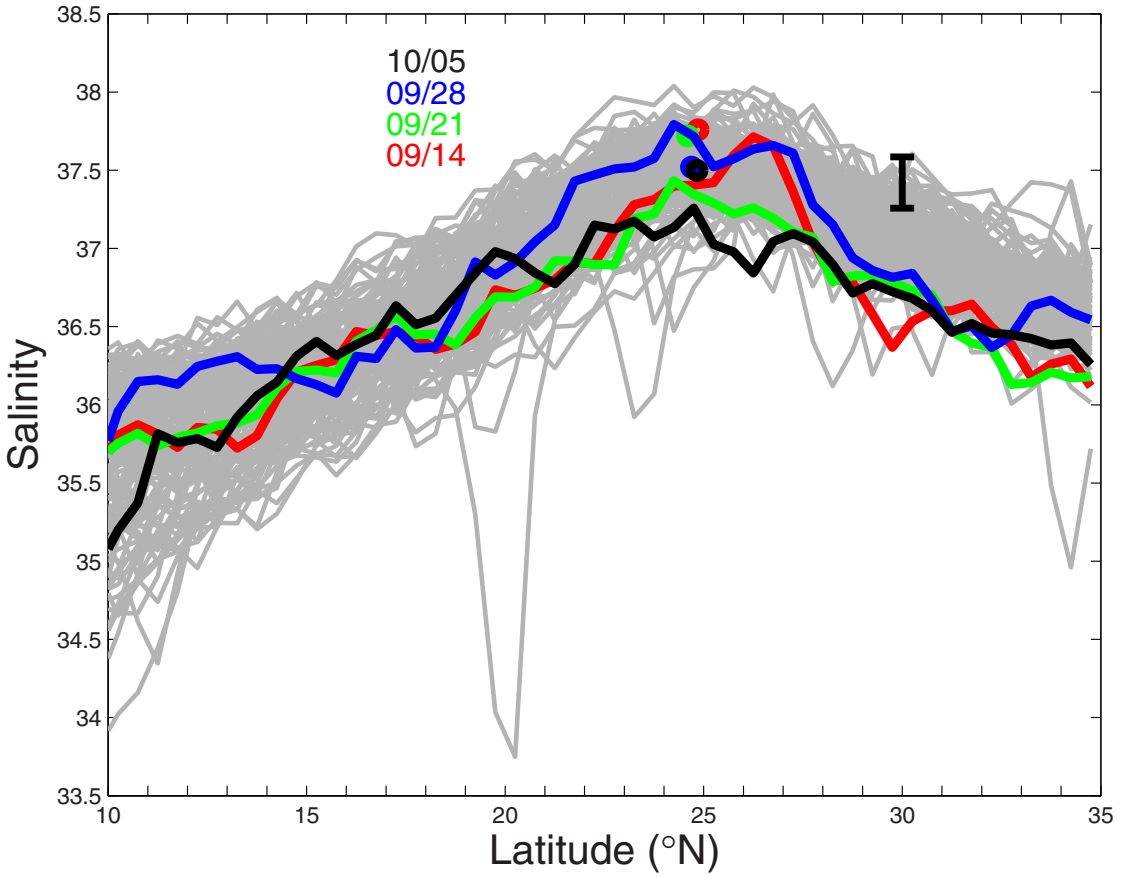

Figure 2. Colored lines: Four realizations of salinity for one particular beam and track. Dates (month/day, 2012) are indicated by colors and matching text labels. Gray lines: all realizations of the same track. The track displayed here is an ascending one that happens to cross directly over the SPURS central mooring at (24.8°N, 38°W). See Figure 1 for location. Also shown are hourly salinity values measured by the mooring from the exact time when the satellite passed over it with color-coded markers for each date (slightly randomized in latitude for clarity). Black bar at 30°N is the mean salinity from the mooring at 24.8°N plus and minus the standard deviation. It was placed at 30°N for clarity.

processed as described in *Delcroix et al.* [2005] and *Reverdin et al.* [2007]. This SOOP data set is objectively mapped onto a 1° × 1° grid and includes archived data up to 2009. Upper ocean (top 30 m) currents come from the OSCAR project [*Bonjean and Lagerloef*, 2002]. The ERAI [*Dee et al.*, 2011] atmospheric reanalysis product is briefly displayed to document surface fluxes of freshwater. The *de Boyer-Montegut et al.* [2004] mixed-layer climatology is used along with the reanalysis products to calculate freshwater forcing. A gridded temperature and salinity product produced from Argo, TAO/Triton and available CTD data, the JAMSTEC MOAA GPV [*Hosoda et al.*, 2008] will be shown to verify year-to-year variability observed in the Aquarius data.

Comparison between the Aquarius data set and the SPURS central mooring over a 1 month period (colored lines and symbols in Figure 2) shows a relatively noisy correspondence between the two data sets. It also shows the spread of observations over a longer time over one beam and one track. We compared SSS data from the mooring over the entirety of the mooring deployment with the closest Aquarius node and found an RMS difference of 0.21. This is within the satellite accuracy stated above, but greater than the value estimated by Y. Chao (personal communication, 2014) also quoted above. One should use caution in directly comparing buoy and Aquarius data at one point like this. The buoy measurements are single point, whereas Aquarius is averaged over a 50–100 km area [*Tang et al.*, 2014].

3. Results

The seasonal variability in the Aquarius data set and SOOP data are mostly similar (Figure 3) but vary somewhat in detail. The maximum latitudinal extent of the 37.4 isohaline as seen in the Aquarius data (Figure 3a)

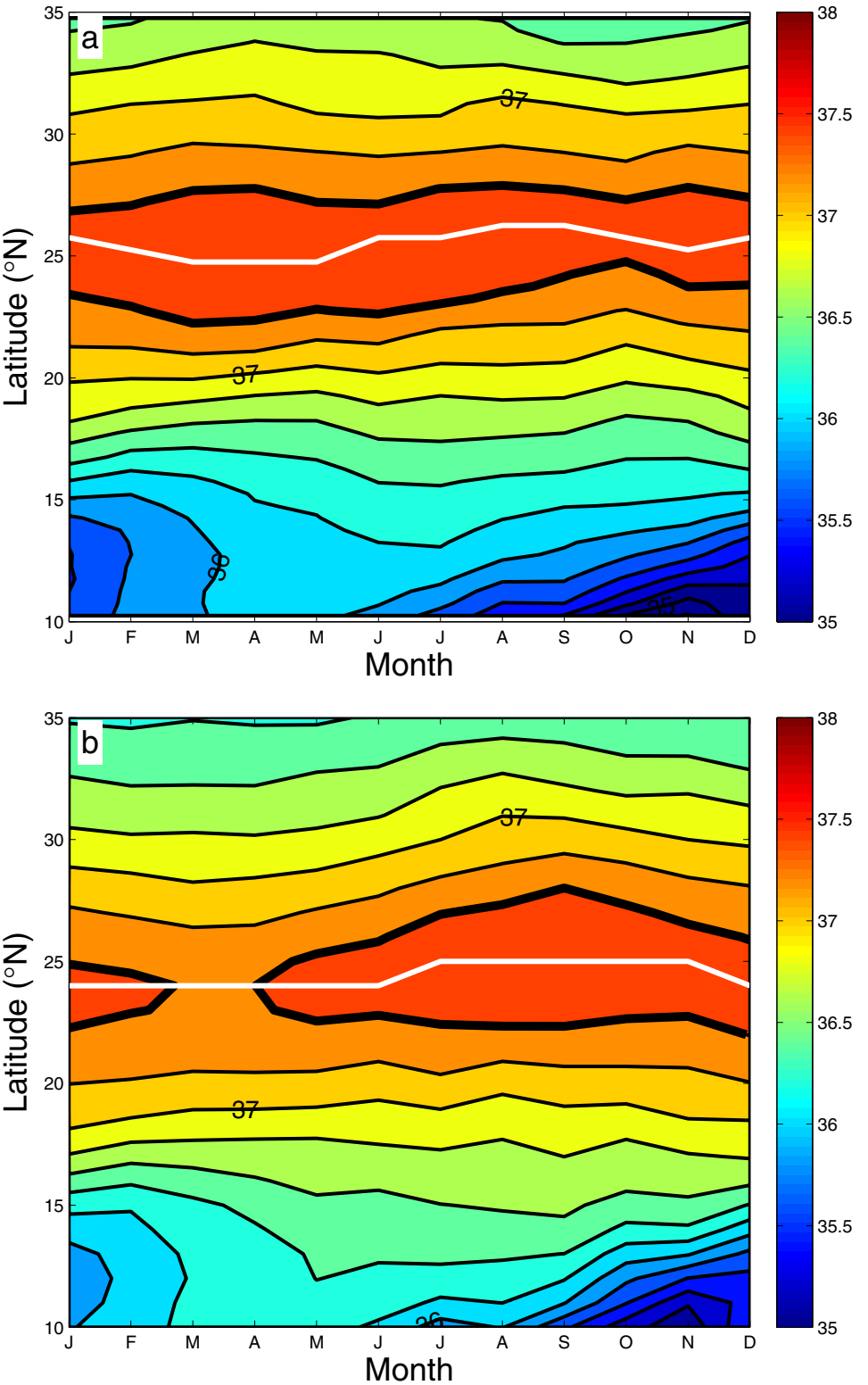

Figure 3. (a) Salinity as a function of latitude averaged for all Aquarius tracks displayed in Figure 1 for different months for the August 2011 to September 2013 period. Color bar at right gives values in salinity units. Contour lines are at intervals of 0.2. Heavy lines are 37.4 contour. White line is the latitude of maximum salinity for each month. (b) As in Figure 3a but using SOOP data averaged in the box (10°N–35°N, 30°W–45°W).

is higher than that seen in the SOOP data (Figure 3b). This could indicate that the 2 years of Aquarius were anomalously salty as the SOOP data used end in 2009. Alternatively it could be an artifact of the 1° × 1° smoothing done on the SOOP data. The 37.4 contour in Figure 3 shows expansion and contraction of the surface area and latitudinal extent of the SSS-max throughout the year that varies between the different data sets. The maximum extent of the SSS-max is in March–April in the Aquarius data and September in the SOOP data. The minimum extent comes in March–April in the SOOP data and in October in the Aquarius data. The north-south motion of the maximum SSS (white line in Figure 3) is similar in the two data sets, with the furthest north extent in September and furthest south in April–May. The difference in seasonality of the extent of the SSS-max between the two data sets may be the result of the location of the ship crossings that comprise most of the SOOP observations, which *Reverdin et al*. [2007] show to be somewhat to the east of the center of the SPURS region.

The mean location of the maximum salinity on each track, indicating the axis of the SSS-max, for the entire extent of the Aquarius data set (Figure 1) slants slightly northeastward in the SPURS region, from 24.5°N to 26.5°N. This may be due to the distribution of Ekman transport by the northeast Trade Winds. Another possible explanation is that coastal upwelling near Africa may impact the SSS-max area more strongly in the east. Or perhaps it is because there is greater evaporation minus precipitation near the African continent (J. D'Addezio and F. M. Bingham, A subtropical North Atlantic regional atmospheric moisture budget, submitted to *Journal of Geographic Research Oceans*, 2014, henceforth DB14). The mean value of the salinity at the maximum, not shown, is a nearly constant 37.8 for all tracks.

The envelope of all salinities measured along one track gives some indication of the along-track variability (Figure 2). Occasional outliers show far greater surface gradients than can be attributed to pure mesoscale stirring on the mean surface fields in this area, and are likely influenced by local rain events. This idea is substantiated by comparison with TRMM precipitation data, which showed rain events to be coincident with some of the largest outliers.

The subtropical North Atlantic has a seasonal cycle in salinity whose size changes with latitude. The size of the seasonal cycle in Figure 3a is largest between 10°N and 15°N. Maximum SSS at 10°N is in April–May and minimum is in November–December. 10°N is just north of the farthest northward seasonal extent of the ITCZ [*Waliser and Gauthier*, 1993]. The large seasonal cycle in SSS at this latitude is mainly forced by seasonally migrating rainfall [*Foltz and McPhaden*, 2008]. Poleward of about 30°N is another area with slightly larger seasonal cycles. A full seasonal budget of the SSS has not been done north of the SSS-max, but it is likely forced by a different mechanism from that south of it, perhaps by seasonal variability of freshwater forcing and Ekman pumping [*Bingham et al*., 2012], but also possibly by horizontal or vertical mixing. As will be discussed below, the lack of a meridional gradient of seasonal phase suggests that meridional advection is not an important part of the seasonal balance north of the SSS-max. From 20°N to 30°N, the contours are relatively horizontal in Figure 3a, meaning weak or nonexistent seasonal cycles likely due to weak variability in the forcing.

To get a view of the seasonal cycle of SSS in more detail, we use harmonic analysis as described in section 2. The amplitude of the seasonal cycle is largest at 10°N, with a value of about 0.4 (Figure 4a). It decreases northward to a minimum at 25°N–30°N and increases a little north of that (Figure 4b). As stated above, at 10°N the maximum SSS is in spring, April–May (Figures 3a, 5a, and 5b). It gets later in the year with increasing latitude, reaching December–January at 20°N and March–April again at 25°N. (The descending tracks in Figure 5a seem to show a more regular pattern in phase than the ascending.) Maximum SSS occurs in April–May north of 30°N (Figure 5b). The phase is fairly coherent between 10°N and about 16°N. North of that, it becomes more scattered, likely due to the fact that the amplitude gets so small, below 0.2 and less than the accuracy of the Aquarius measurement, that the phase becomes more difficult to determine. Note that Figure 5a appears very similar to the results of *Dessier and Donguy* [1994, Figure 2B].

The meridional location of the maximum SSS varies by date (white line in Figures 3a and 6a). It has migrated north and south over the course of the Aquarius mission, with a mainly seasonal component to its movement. It was farthest north in September 2011, August 2012, and August 2013 and farthest south in February–March 2012 and May 2013. The range of the migration is about 2° in latitude, 24.25°N–26.25°N. The maximum salinity along each track (Figure 6b) has variability too, but it is not seasonal in nature. It ranges from 37.8 down to less than 37.6. The decrease between July 2012 and January 2013 agrees with most observations taken during the SPURS field program, which took place in this area during this time period.

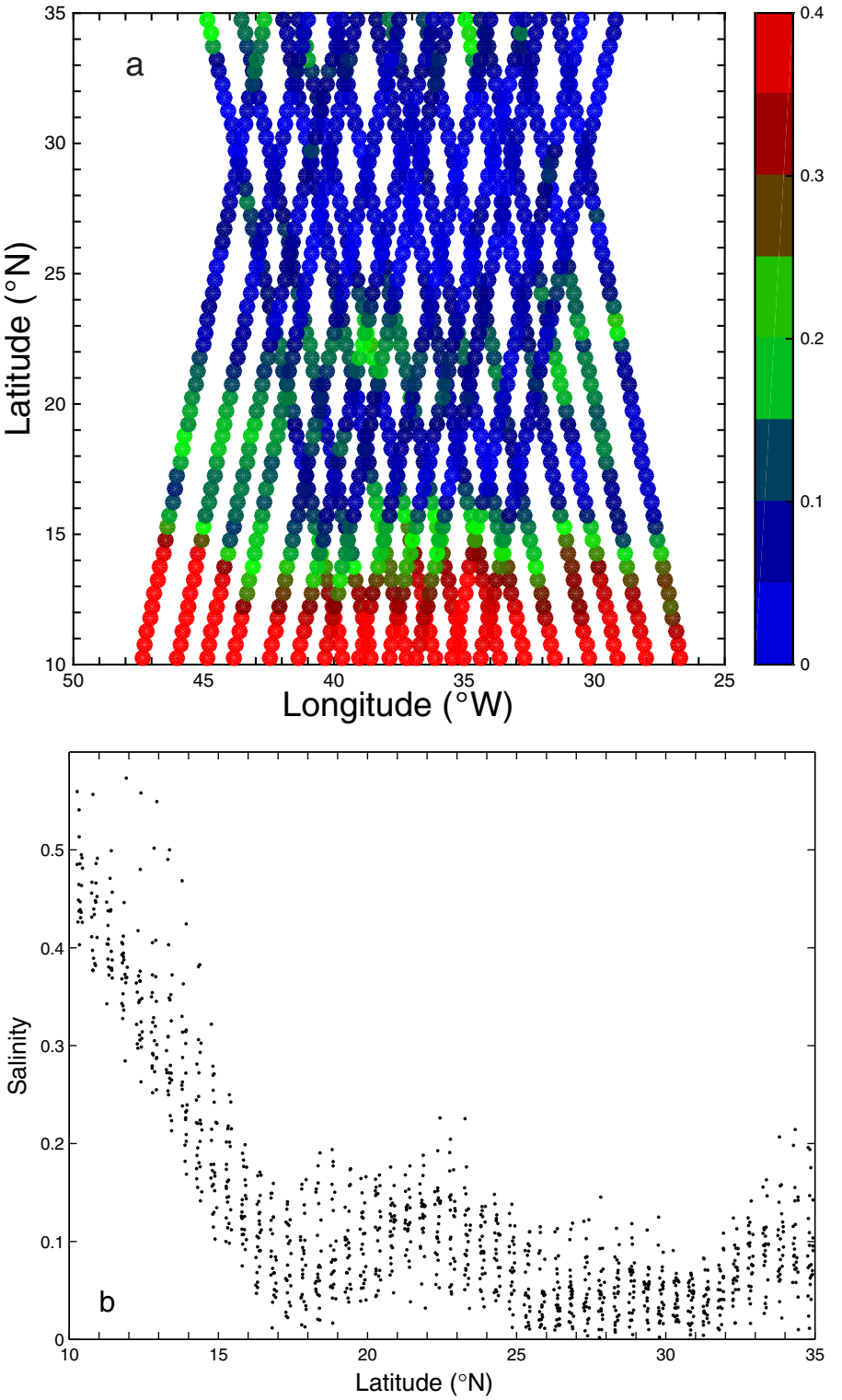

Figure 4. (a) Amplitude of the seasonal harmonic of SSS. Color scale is at right in unitless practical salinity. (b) Amplitude of the seasonal harmonic of SSS as a function of latitude. Each dot represents the seasonal cycle at one node. Latitude positions are slightly displaced by a random amount for clarity.

The evaporation minus precipitation averaged over the SPURS region (E-P; Figure 7) has seasonal variation, ranging from 1 mm/d in November 2012 up to 5–6 mm/d in March 2012. The minimum is in late fall corresponding to a peak in rainfall associated with Saharan air layer intrusions over the eastern North Atlantic

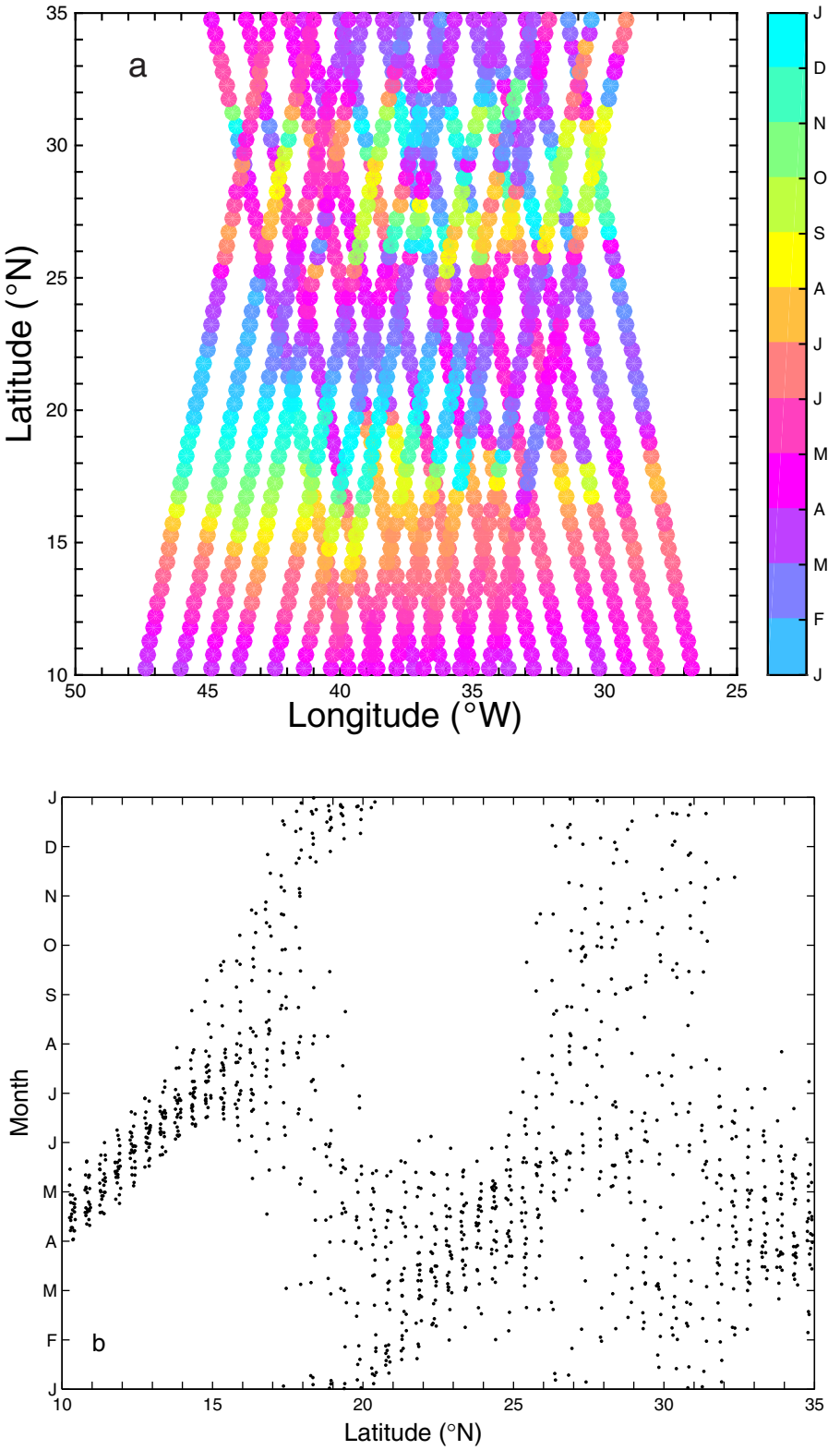

Figure 5. (a) Phase of the seasonal harmonic of SSS. Color scale is at right indicating month of maximum salinity. (b) Phase of the seasonal harmonic of SSS as a function of latitude. Each dot represents the seasonal cycle at one node. Latitude positions are slightly displaced by a random amount for clarity.

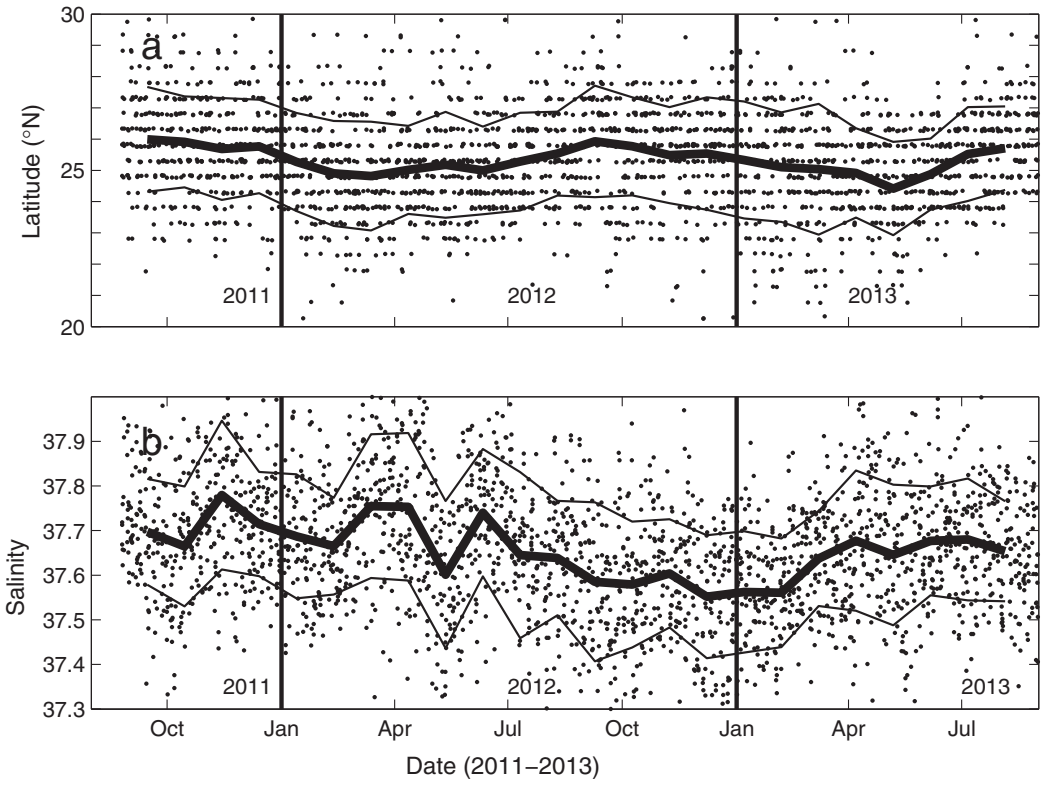

Figure 6. (a) Latitude of the maximum salinity along each track as a function of date. Heavy curve is a monthly average. Light curves are the monthly average plus or minus monthly standard deviations. Dots are from individual satellite passes, with positions slightly randomized for clarity. (b) As in Figure 6a, but for salinity at the salinity maximum.

[*Dunion and Velden*, 2004]. The mean seasonal E-P in the SPURS region (not shown) has a maximum in January of about 4.3 mm/d and a minimum in September of 2.5 mm/d (DB14). The fall of 2012 thus had an abnormally low E-P, possibly due to rainfall from the four tropical systems that passed through the area during that time. This low E-P matches the timing of the observed decrease in salinity (Figure 6b). Whether there was enough precipitation to cause this observed change is a subject for future study.

The surface freshwater forcing describing the change in SSS due to surface flux is S_0(E-P)/h, where S_0 is a reference salinity, and h is the mixed-layer depth [*Delcroix et al*., 1996]. With the different phasing of E-P and h, the seasonal cycle of freshwater forcing is modified from that of E-P alone (Figure 7, green curve). Freshwater forcing has a well-defined seasonal cycle, with maximum in the summer in the SPURS region mainly due to thinning of the surface mixed layer. The average surface freshwater forcing in this region from Figure 7 is about 1/yr. The average from DB14 is also about 1/yr. So the mean freshwater forcing during the 2011–2013 was about the same as normal. However, the fall of 2012 had a short period of weaker than normal freshwater forcing (or greater precipitation), the minimum seen in October–December 2012. The minimum in Figure 7, about 0.1/yr, is less than the average minimum fall value of about 0.6/yr. The maximum, in July of each year, was close to normal.

The distribution of frontal features seen in the Aquarius data depends on the scale of the feature. In Figure 8a, the black bar shows the distribution of fronts with small spatial scale, less than the beam separation of about 100 km, whereas the red bars show those with longer scale, 300 km or more. The small fronts have a sharp minimum in the SSS-max, between 23°N and 26°N. These along track changes can generally be an indication of fronts and eddies, areas of enhanced horizontal stirring, confluence of water masses and potential downwelling and local rainfall events. The larger fronts appear near the ITCZ at 10°N–12°N, but are uniformly rare north of that.

The variability of salinity as expressed by the standard deviation (Figure 8b) decreases from 0.6 at 10°N, down to a minimum of 0.2 at 26°N. Large excursions seen in individual tracks are results of single low

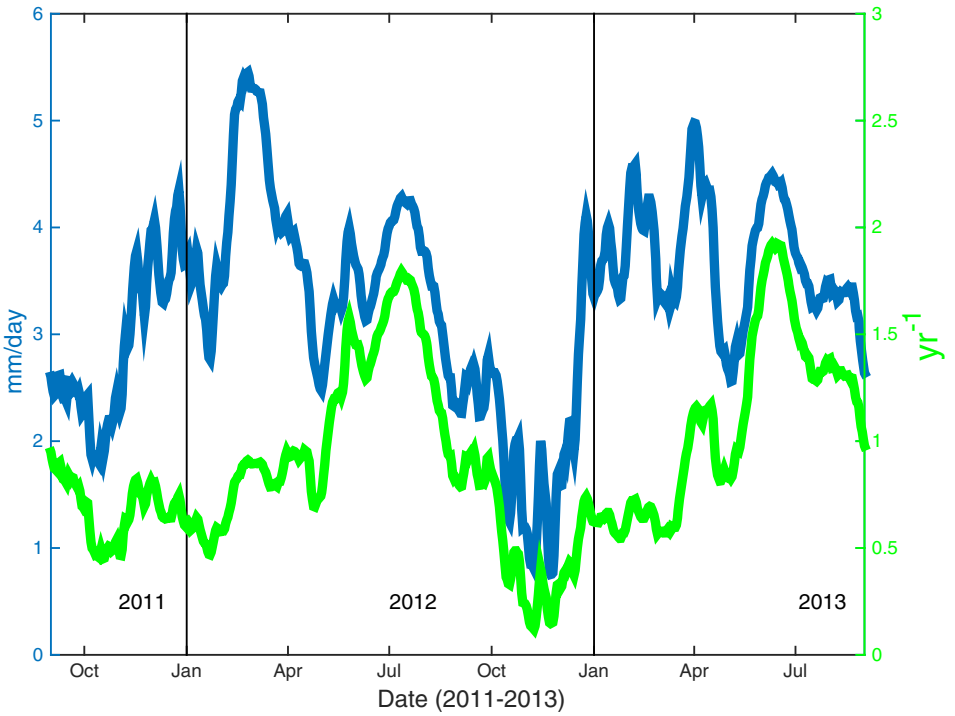

Figure 7. Blue line and left axis. Evaporation minus precipitation (E-P) averaged over the SPURS region calculated from ERAI reanalysis data [*Dee et al.*, 2011]. Green line and right axis. Surface freshwater forcing, S0(E-P)/h, averaged over the same region. S0 is a reference salinity, and h is the mixed-layer depth taken from the *de Boyer-Montegut et al.* [2004] climatology. See DB14 for details of the calculation. A 31 day running mean filter has been applied to both series displayed. We note that DB14 have done the same calculation with the MERRA reanalysis product [*Rienecker et al.*, 2011]. The two products give similar results, though not for this time period (MERRA ends in October 2011). E-P from the two products has a correlation of 0.92.

outliers (e.g., Figure 2). A check of these low outliers indicated that they were indeed low, but not unphysical and could not be eliminated in an ad hoc manner. As stated above, outliers as large as 0.6 may be more likely caused by heavy rain events than advection or eddy stirring on the mean lateral salinity gradient [*Busecke et al.*, 2014]. One has to go quite a ways further south to find water with salinity as low on average as 0.6 less than that of the SSS-max. So the latitudinal maximum of SSS is coincident with the north-south minimum in variance and the north-south minimum of probability of finding fronts or anomalous low-salinity features.

The area of the SSS-max, as defined by the 37.4 isohaline, also varies over the course of the Aquarius data set (Figure 9), from about 0.9×10^6 km^2 in May 2012 to 0.3×10^6 km^2 in October 2012, a decrease of 67%. This plot of area has some similarity to the one of maximum SSS (Figure 6b), with maxima and minima at about the same time.

Taking the difference between the year-long periods (September 2012 to September 2013) and (September 2011 to September 2012), we find large scale differences between them of up to 0.3 in the SPURS region (Figure 10), with the latter period being fresher. This is consistent with Figures 6b and 9. Note that the magnitude of the change is relatively small at 25°N, the latitude of maximum SSS.

4. Discussion

The region just south of the latitudinal maximum of SSS (20°N–24°N) has the characteristics of a small seasonal cycle, a relative paucity of large-scale frontal features, relatively little change over the course of the Aquarius mission and small variance relative to the surrounding regions. It should be noted that this statement applies to Aquarius data, but not necessarily in situ data, which may show more variability at small spatial and short time scales than the satellite is capable of resolving. Potential irregularities in the seasonal cycle, which has only been observed twice by Aquarius, may also be a factor. What does this tell us about

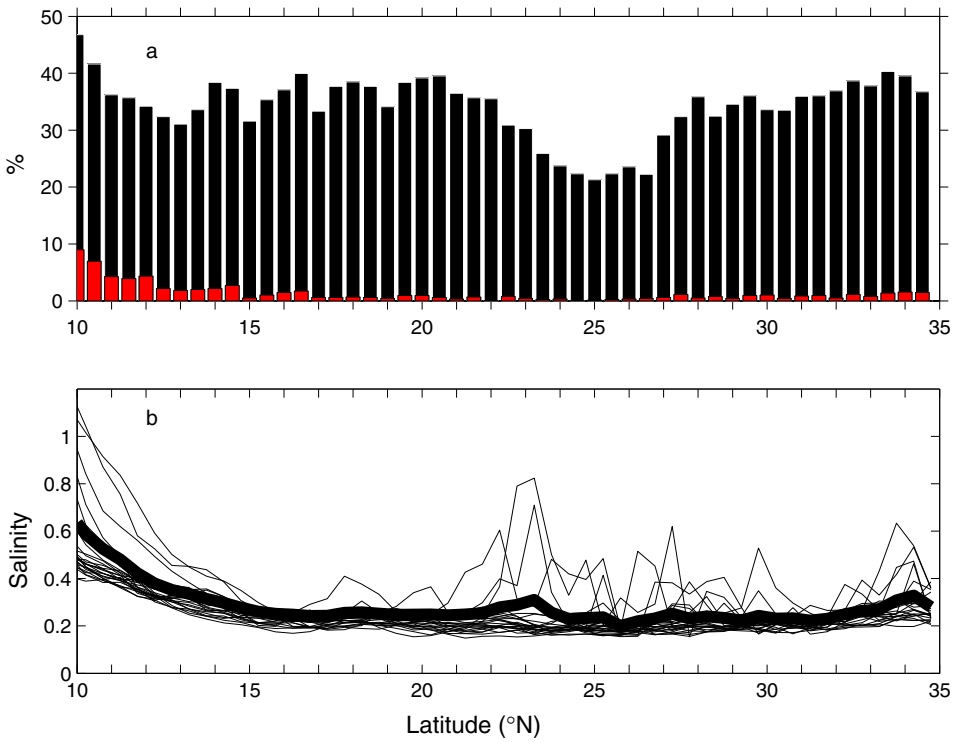

Figure 8. (a) Probability of finding fronts in %. A front is defined as an along-track change in salinity from an individual Aquarius pass of more than 0.2 of either sign. Black bars: The points included here are ones where there was a salinity change in any beam. Red bars: The points included here are ones where there was a salinity change in all three beams at once. (b) Standard deviation of salinity as a function of latitude for the Aquarius data set, eight tracks, three beams/track. Light black curves are from individual tracks and beams. Heavy curve is the standard deviation from all tracks and beams put together.

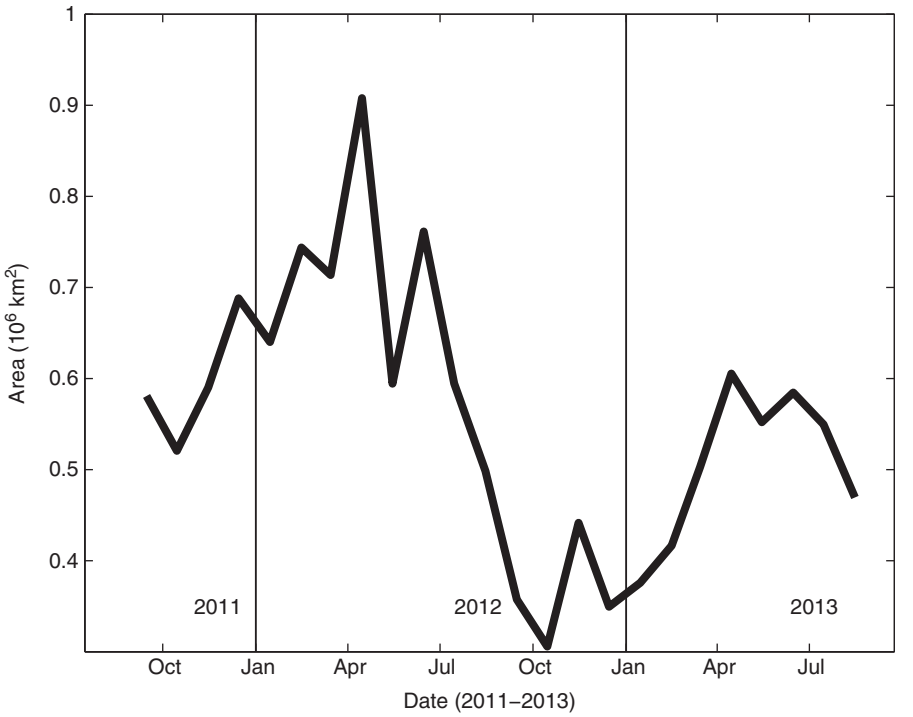

Figure 9. Surface area of SSS-max, defined as SSS > 37.4. Area is calculated from ascending passes only (the same calculation from the descending passes yielded similar results). Curve is a monthly average.

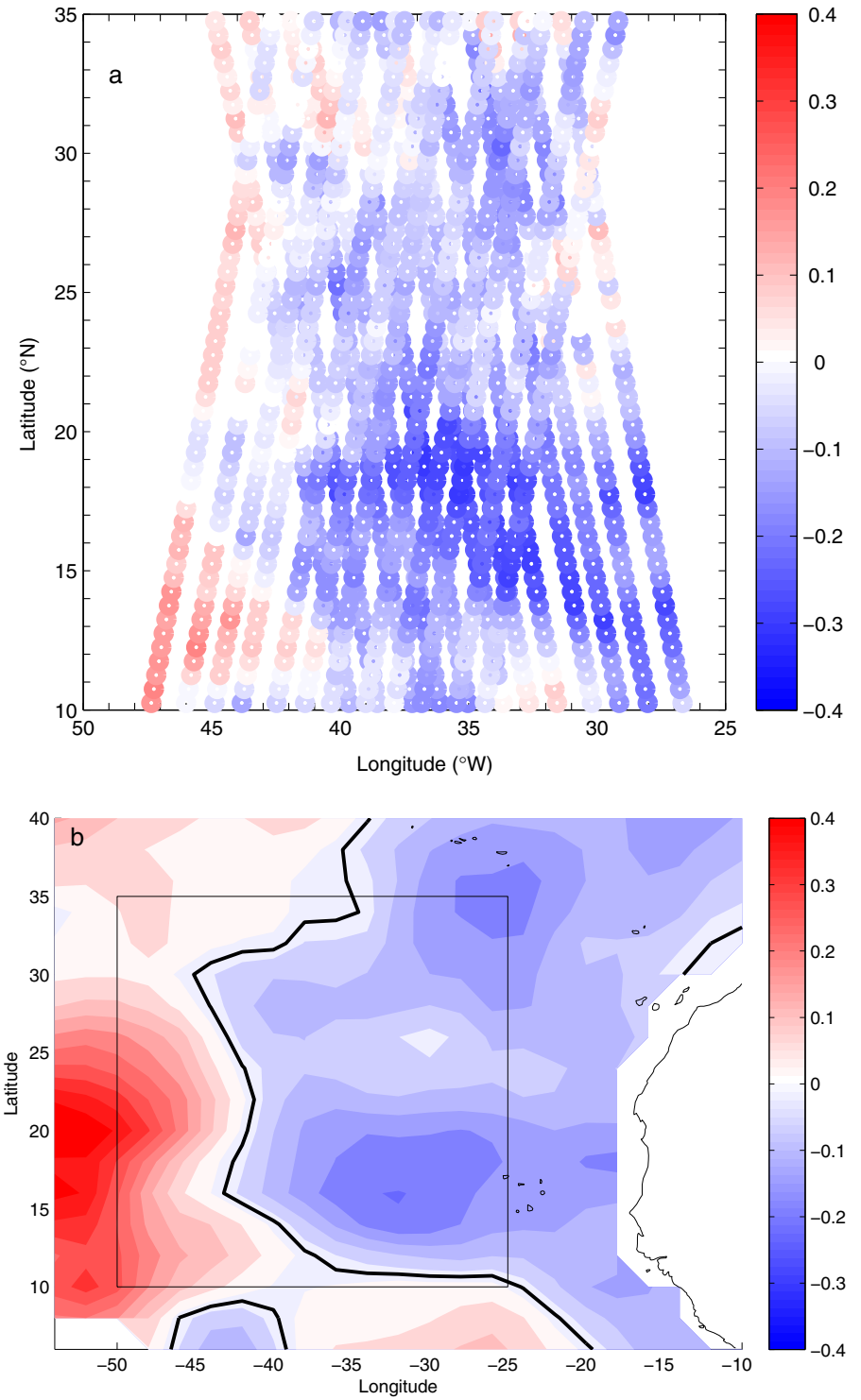

Figure 10. (a) Near-surface salinity difference between the (September 2012 to August 2013) and (September 2011 to August 2012) means from Aquarius data. (b) As in Figure 10a, but the data used to produce it are taken from the MOAA GPV Argo product (see section 2). Black box in Figure 10b is the outline of the plotbox of Figure 10a.

the processes by which the SSS-max is formed and maintained? In the classical view, surface water undergoes mean Ekman transport to the north-northwest under a regime of strong atmospheric divergence of moisture, i.e., large E-P. Evaporation, the dominant process acting on the surface waters, is slow and removes freshwater as surface water moves poleward. In the SSS-max and just north of it, northward

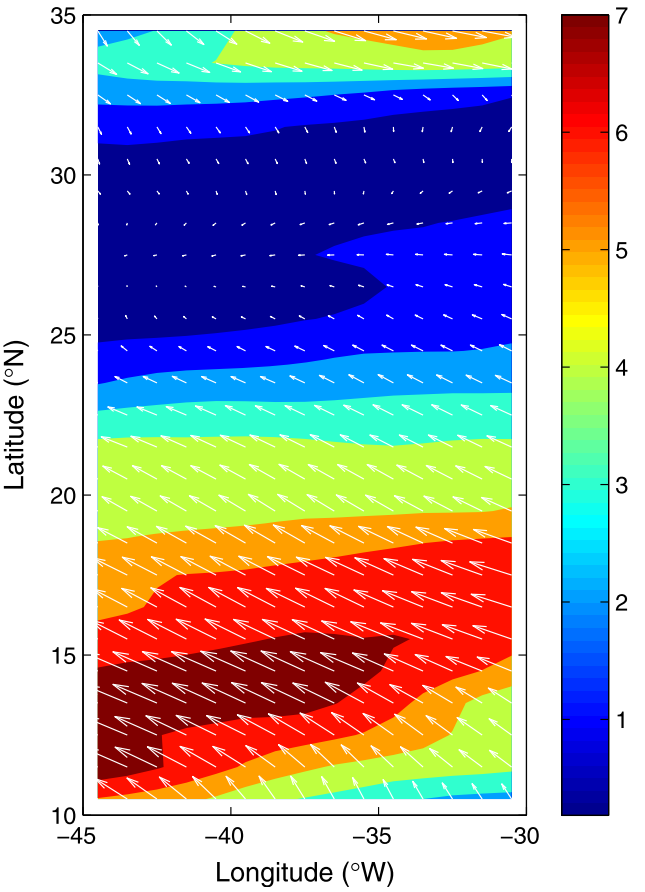

Figure 11. Mean (1993–2012) surface velocity from the OSCAR (ocean surface current analysis real-time) data. Color indicates speed with scale at right in cm/s. Overlain arrows show direction and speed.

motion comes to a stop (Figure 11), generating convergence and subduction. Thus, the data presented here are consistent with the classical understanding of the SSS-max. Figure 11 is also evidence for the greater importance of the northward-flowing part of the converging flow shown by *Gordon and Giulivi* [2014], as opposed to southward transport from the northern part of the subtropical gyre [*Qu et al*., 2013]. The SSS-max is situated just at the northern edge of the flow from the tropics, where it comes to a stop. The line of maximum SSS (Figure 1) even trends northeastward like the speed contours in Figure 11.

Busecke et al. [2014] and *Gordon and Giulivi* [2014] emphasize the northward transport of fresh water into this region as an eddy-driven process. Filaments of fresh water move northward in a turbulent flow field, originating from areas of stronger eddy kinetic energy to the south and west of the SSS-max. Mesoscale turbulence plays an important role in setting mixed layer properties. During the SPURS cruises of 2012 and 2013, a number of such fresh filaments were observed entering the area and covering over the high salinity layer at the surface (R. Schmitt and J. Font, personal communication) an example of which is shown by *Busecke et al*. [2014]. Ekman transport creates and maintains large-scale gradients which are necessary for eddy fluxes and may even control the amount of eddy activity by influencing the horizontal density gradients and consequent baroclinic instability. *Cessi* [2007] noted that Ekman pumping can introduce available potential energy on which eddies can grow.

One surmises from the close correspondence between the structure of the seasonal cycle of SSS and the location of the maximum SSS (Figures 1, 3a, and 4–6a) that seasonal processes are a signature of the maintenance of the SSS-max and an integral part of its formation. Strong seasonal variability is imposed upon the surface waters under the ITCZ by seasonally varying rainfall which attains its farthest northward extent at 8°N–10°N in August–September [*Waliser and Gauthier*, 1993]. Maximum SSS under the ITCZ at 8°N–10°N occurs in March–April (Figure 3) and minimum in November. As those waters move northward under the influence of trade wind-driven Ekman transport the observed date of maximum SSS increases with latitude (Figures 3a and 5b) and the amplitude of the seasonal cycle decreases (Figures 3a and 4b) en route. The seasonal variability of the region near the ITCZ was nicely detailed by *Grodsky et al*. [2014]. They describe an alternating SSS maximum and minimum that develops around 10°N driven by the combination of seasonal variability in the Amazon River outflow, seasonal changes in the retroflection of the North Brazil Current, and seasonal migration of the ITCZ. The most important terms in the mixed layer salt budget at 10°N–15°N are vertical diffusion, meridional advection, and surface flux. Essentially what we are seeing in the SPURS region is eddy-driven processes marking the northward extension of that variability. As the water moves northward, advection decreases and evaporation increases.

The mean flow in the subtropical North Atlantic (Figure 11) reveals that a typical magnitude of the northward component of current between 10°N and 20°N is about 5 cm/s, including both Ekman and

geostrophic components. This means a time of 8–9 months required for water to travel from 10°N to 20°N, which matches well with the phase propagation implied in Figure 5b. When the surface water reaches a latitude of ~25°N, northward flow mostly stops, as Ekman transport is balanced by the slow background geostrophic flow to the south or southwest [*Reid*, 1978, 1994]. Combining values of surface flux (Figure 7) and velocity (Figure 11), DB14 estimate the change in mixed-layer salinity between 15°N and 25°N to be about 0.6, about 1/3–1/2 of the observed value. This leaves other processes such as local evaporation, subduction, and vertical and horizontal mixing to account for the rest of the change.

Throughout the subtropical ocean seasonal subduction removes water from the surface layer and injects it into the interior circulation [*Qiu and Huang*, 1995], with the process being strongest in winter. At 25°N this results in the formation of the STUW. Thus, the structure and strength of the Ekman transport, the timing of the seasonal cycle of SSS in the ITCZ and the North Brazil Current retroflection and the timing of subduction processes at 25°N all contribute to the formation and maintenance of the SSS-max and the STUW, making it a compact and recognizable feature. The fact that there is relatively little seasonal variability in the SSS-max helps to give STUW its relative stability in water properties.

A surprising aspect of the analysis here is the nonseasonal variability shown in Figures 6b, 9, and 10. It has not been possible to document such changes to this major ocean feature in such detail until the advent of the Aquarius observations. The freshening from 2012 to 2013 indicated in Figure 10, along with the change in area (Figure 9) and maximum SSS (Figure 6b), raise significant questions about which processes control the interannual variability in the region. Is it a result of changes in surface freshwater flux, subduction rates, mixed layer depths, gyre-scale circulation, Ekman transport or horizontal or vertical mixing? How will it impact the interior circulation as subducted water becomes fresher? Is this variability significant compared to other years? None of these items can be determined using the Aquarius data set alone, and thus definitive answers are subjects for future research. Although the entire SPURS region showed decreasing salinity during the Aquarius era, the fastest decrease was around 15°N (Figure 10), south of the SSS-max, at a rate approaching −0.3/yr. The southern part of the SPURS region is the source for the northern part. So it is possible that the decrease we see is not so much related to processes in and around the SSS-max, but changes of rainfall within the ITCZ, the eddy kinetic energy and the consequent turbulent flux, the slow mean Ekman transport [*Chereskin and Roemmich*, 1991; *Price et al*., 1987], the retroflection of the North Brazil current or the outflow of the Amazon river [*Grodsky et al*., 2014]. These possible changes might be related to the larger-scale circulation and variability of the tropical Atlantic and even the global ocean-atmosphere system.

What are the implications of the seasonal and nonseasonal variability we have detailed above for the downstream properties of STUW and the circulation of the upper ocean? This question is complicated, because the downstream properties of STUW depend on a number of factors besides just the salinity of the source water, mainly the strength of subduction, the strength and type of mixing, and the configuration of the interior flow [*Bingham et al*., 2002; *Bauer and Siedler*, 1988; *Johnson and McPhaden*, 1999]. In this work, we have observed changes in the SSS-max, particularly in the area and maximum SSS. Assuming all else remains the same, as the SSS-max water gets saltier subducted water will get saltier too, and consequently denser. As this change propagates into the interior circulation of the upper ocean it may increase stratification in the tropical thermocline and make vertical processes less efficient. As vertical diffusion is one of the most important means by which freshwater is removed from the surface layer [*Grodsky et al*., 2014; *Foltz and McPhaden*, 2008] this could have the effect of further increasing the stratification. At the same time, as more freshwater remains in the surface layer and is advected northward toward the SSS-max, the effect would be to decrease the SSS in the SSS-max. As the water in the SSS-max gets saltier, it also gets denser which may result in an acceleration of the subtropical cell, and greater northward surface transport of fresh water. So in this sense, the SSS-max may be self-stabilizing, a negative feedback loop. Perhaps this helps explain the presence of a similar feature in almost every ocean basin (Gordon et al., Variability within the salty subtropical oceanic regions, submitted to *Oceanography*, 2014).

Acknowledgments

Support was provided by NASA under grants NNX09AU70G and NNX11AE83G to UNCW and NNX09AU68G to Lamont-Doherty Earth Observatory. Three anonymous reviewers read this manuscript carefully and provided constructive comments. The SPURS central mooring observations were supported by NASA grant NNX11AE84G. Figure 7 data were provided by J. D'Addezio. Lamont-Doherty Earth Observatory contribution 7838. The gridded sea surface salinity (SOOP) data set was made freely available by the French Sea Surface Salinity Observation Service. Data were obtained from the following sources: Aquarius data (PO.DAAC data archive), http://podaac.jpl.nasa.gov; SOOP data, http://www.legos.obs-mip.fr/observations/sss/; JAMSTEC MOAA GPV, http://www.jamstec.go.jp/ARGO/argo_web/MapQ/Mapdataset_e.html; SPURS Central mooring data, http://uop.whoi.edu/projects/SPURS/spurs.html; ERAI data, https://climatedataguide.ucar.edu/climate-data/era-interim; Mixed-layer depth climatology, http://www.ifremer.fr/cerweb/deboyer/mld/home.php.

References

Bauer, E., and G. Siedler (1988), The relative contributions of isopycnal and diapycnal mixing below the subtropical salinity maximum, *Deep Sea Res., Part A*, *35*, 811–837.

Bingham, F. M., T. Suga, and K. Hanawa (2002), The origin of waters observed along 137°E, *J. Geophys. Res.*, *107*(C7), 3073, doi:10.1029/2000JC000722.

Bingham, F. M., G. R. Foltz, and M. J. McPhaden (2010), Seasonal cycles of surface layer salinity in the Pacific Ocean, *Ocean Sci.*, *6*, 775–787, doi:10.5194/os-6-775-2010.
Bingham, F. M., G. R. Foltz, and M. J. McPhaden (2012), Characteristics of the seasonal cycle of surface layer salinity in the global ocean, *Ocean Sci.*, *8*, 915–929, doi:10.5194/os-8-915-2012.
Bonjean, F., and G. S. Lagerloef (2002), Diagnostic model and analysis of the surface currents in the Tropical Pacific Ocean, *J. Phys. Oceanogr.*, *32*, 2938–2954.
Busecke, J., A. L. Gordon, Z. Li, F. M. Bingham, and J. Font (2014), Subtropical surface layer salinity budget and the role of mesoscale turbulence, *J. Geophys. Res. Oceans*, *119*, 4124–4140, doi:10.1002/2013JC009715.
Cessi, P. (2007), Regimes of thermocline scaling: The interaction of wind stress and surface buoyancy, *J. Phys. Oceanogr.*, *37*, 2009–2021.
Chereskin, T. K., and D. Roemmich (1991), A comparison of measured and wind-derived Ekman Transport at 11°N in the Atlantic Ocean, *J. Phys. Oceanogr.*, *21*, 869–878.
de Boyer-Montegut, C., G. Madec, A. S. Fischer, A. Lazar, and D. Iudicone (2004), Mixed layer depth over the global ocean: An examination of profile data and a profile-based climatology, *J. Geophys. Res.*, *109*, C12003, doi:10.1029/2004JC002378.
Dee, D. P., et al. (2011), The ERA-Interim reanalysis: Configuration and performance of the data assimilation system, *Q. J. R. Meteorol. Soc.*, *137*, 553–597, doi:10.1002/qj.828.
Delcroix, T., et al. (1996), Precipitation and sea-surface salinity in the Tropical Pacific, *Deep Sea Res., Part I*, *43*(7), 1123–1141.
Delcroix, T., A. Dessier, Y. Gouriou, and M. McPhaden (2005), Time and space scales for sea surface salinity in the tropical oceans, *Deep Sea Res. Part I*, *52*, 787–813.
Dessier, A., and J. R. Donguy (1994), The sea surface salinity in the Tropical Atlantic between 10°S and 30°N—Seasonal and interannual variations (1977–1989), *Deep Sea Res., Part I*, *41*(1), 81–100.
Dunion, J. P., and C. S. Velden (2004), The impact of the Saharan air layer on Atlantic tropical cyclone activity, *Bull. Am. Meteorol. Soc.*, *85.3*, 353–365.
Emery, W. J., and R. E. Thomson (2001), *Data Analysis Methods in Physical Oceanography*, 2nd ed., 658 p., Elsevier Sci., Oxford, U. K.
Foltz, G. R., and M. J. McPhaden (2008), Seasonal mixed layer salinity balance of the tropical North Atlantic Ocean, *J. Geophys. Res.*, *113*, C02013, doi:10.1029/2007JC004178.
Gordon, A. L., and C. F. Giulivi (2014), Ocean eddy freshwater flux convergence into the North Atlantic subtropics, *J. Geophys. Res. Oceans*, *119*, 3327–3335, doi:10.1002/2013JC009596.
Grodsky, S. A., J. A. Carton, and F. O. Bryan (2014), A curious local surface salinity maximum in the Northwestern Tropical Atlantic, *J. Geophys. Res. Oceans*, *119*, 484–495, doi:10.1002/2013JC009450.
Hosoda, S., T. Ohira, and T. Nakamura (2008), A monthly mean dataset of global oceanic temperature and salinity derived from Argo float observations, *JAMSTEC Rep. Res. Dev.*, *8*, 47–59.
Johnson, G. C., and M. J. McPhaden (1999), Interior pycnocline flow from the subtropical to the equatorial Pacific Ocean, *J. Phys. Oceanogr.*, *29*, 3073–3089.
Lagerloef, G. S., et al. (2008), The Aquarius/SAC-D Mission: Designed to meet the salinity remote-sensing challenge, *Oceanography*, *20*(1), 68–81.
Lagerloef, G. S., et al. (2013), Aquarius salinity validation analysis, Data Version 2.0, technical report, Aquarius Project document AQ-014-PS-0016, Aquarius SAC/D, Seattle, Wash.
McCreary, J., and P. Lu (1994), On the interaction between the subtropical and equatorial ocean circulations: The subtropical cell, *J. Phys. Oceanogr.*, *24*, 466–497.
Mourre, B., J. Ballabrera-Poy, E. García-Ladona, and J. Font (2008), Surface salinity response to changes in the model parameters and forcings in a climatological simulation of the eastern North-Atlantic Ocean, *Ocean Modell.*, *23*(1–2), 21–32, doi:10.1016/j.ocemod.2008.03.002.
O'Connor, B. M., R. Fine, and D. Olson (2005), A global comparison of subtropical underwater formation rates, *Deep Sea Res., Part I*, *52*(9), 1569, doi:10.1016/j.dsr.2005.1501.1011.
PO.DAAC (2014), Aquarius user guide: Aquarius Version 3.0, technical report, Document # JPL D-70012, AQ-010-UG-0008, 86 p., Phys. Oceanogr. Distrib. Activ. Arch. Cent., Jet Propul. Lab., Pasadena, Calif.
Price, J. F., R. A. Weller, and R. R. Schudlich (1987), Wind-driven ocean currents and Ekman transport, *Science*, *238*, 1534–1538.
Qiu, B., and X. Huang (1995), Ventilation of the North Atlantic and North Pacific: Subduction versus obduction, *J. Phys. Oceanogr.*, *25*, 2374–2390.
Qu, T., S. Gao, and I. Fukumori (2011), What governs the North Atlantic salinity maximum in a global GCM?, *Geophys. Res. Lett.*, *38*, L07602, doi:10.1029/2011GL046757.
Qu, T., S. Gao, and I. Fukumori (2013), Formation of salinity maximum water and its contribution to the overturning circulation in the North Atlantic as revealed by a global general circulation model, *J. Geophys. Res. Oceans*, *118*, 1982–1994, doi:10.1002/jgrc.20152.
Reid, J. L. (1978), On the middepth circulation and salinity field in the North Atlantic Ocean, *J. Geophys. Res.*, *83*(C10), 5063–5067.
Reid, J. L. (1994), On the total geostrophic circulation of the North Atlantic Ocean: Flow patterns, tracers and transports, *Prog. Oceanogr.*, *33*, 1–92.
Reverdin, G., E. Kestenare, C. Frankignoul, and T. Delcroix (2007), Surface salinity in the Atlantic Ocean (30°S–50°N), *Prog. Oceanogr.*, *73*, 311–340, doi:10.1016/j.pocean.2006.11.004.
Rienecker, M. M., et al. (2011), MERRA: NASA's modern-era retrospective analysis for research and applications, *J. Clim.*, *24*, 3624–3648, doi:10.1175/JCLI-D-11-00015.1.
Roemmich, D., et al. (2001), Argo: The global array of profiling floats, in Observing the Oceans in the 21st Century: a Strategy for Global Ocean Observations, edited by N. R. Smith and C. J. Koblinsky, pp. 248–258, CSIRO Publishing, Hobart, Tasmania.
Talley, L. D., G. L. Pickard, W. J. Emery, and J. H. Swift (2011), *Descriptive Physical Oceanography: An Introduction*, 6th ed., 555 p., Elsevier, Amsterdam.
Tang, W., S. H. Yueh, A. G. Fore, and A. Hayashi (2014), Validation of Aquarius sea surface salinity with in situ measurements from Argo floats and moored buoys, *J. Geophys. Res. Oceans*, *119*, 6171–6189, doi:10.1002/2014JC010101.
Waliser, D. E., and C. Gauthier (1993), A satellite-derived climatology of the ITCZ, *J. Clim.*, *6*, 2162–2174, doi:10.1175/1520-0442(1993)006<2162:ASDCOT>2.0.CO;2.
Worthington, L. (1976), The Johns Hopkins Oceanographic Studies, in *On the North Atlantic Circulation*, edited by R. S. Arthur, D. E. Carritt, R. B. Montgomery, D. W. Pritchard and R. O. Reid, vol. 6, 110 pp., Johns Hopkins University Press, Baltimore.
Zhang, D., M. J. McPhaden, and W. E. Johns (2003), Observational evidence for flow between the subtropical and tropical Atlantic: The Atlantic tropical cells, *J. Phys. Oceanogr.*, *33*, 1783–1797.

Erratum

In the originally published version of this article, Figures 4a and 5b were missing color bars. This error has since been corrected and this version may be considered the authoritative version of record.